Theses and Dissertations

2018

Mechanoregulation Modeling of Bone Healing in Realistic Fracture Geometries

Tianyi Ren
Lehigh University, tianyiren1993@gmail.com

Mechanoregulation Modeling of Bone Healing in Realistic Fracture Geometries

by

Tianyi Ren

Presented to the Graduate and Research Committee
of Lehigh University
in Candidacy for the Degree of
Master of Science
In
Mechanical Engineering and Mechanics

Lehigh University

December 2018

This thesis is accepted and approved in partial fulfilment of the requirements for the degree of Master of Science in Mechanical Engineering.

_____
Date

_____
Dr. Hannah Dailey, Thesis Advisor

_____
Prof. D. Gary Harlow, Chairperson of
Department of Mechanical Engineering and Mechanics

III

Acknowledgements

First and foremost, I wish to thank my advisor, professor Hannah Dailey for her tremendous academic support during the year since I joined the Lab. Her instructive advice and useful suggestions helped me get over all the obstacles I have met when I was writing the thesis. My research would have been impossible without her help.

I would like to thank for the aid and support from Peter Schwarzenberg, who gives me lots of inspirations during my research.

Finally, but by no means least, thanks go to my parents for almost unbelievable support and love.

Table of Contents

List of Tables

List of Figures

Abstract

One of the unique properties of fracture healing is that bones heal by producing new tissues that eventually become indistinguishable from the original ones in the pre-injury state, through the process of tissue differentiation. This process is fundamentally controlled by the mechanical conditions at the fracture site, particularly mechanical strain. Numerical models with strain-based fuzzy logic rules have been successfully applied to simulate bone healing in response to local mechanical stimuli for simple axisymmetric fracture geometries. However, these simplified models were not designed to replicate *in vivo* observations such as delays in healing with torsional instability or anticipated differences in healing rate between different fracture types. Accordingly, the purpose of this work was to apply fuzzy logic mechanoregulation fracture healing simulation techniques to 3D models representing a wider range of clinical fracture geometries under multi-axial loading conditions representative of clinical intramedullary nail fixation. Normalized virtual torsional rigidity of the fracture bone were used in the model to provide the structural measure to track the percentage of healing each patient had undergone.

The results of the strain-based mechnoregultaion models showed that the rate of healing depends on the geometry of the fracture, but that all fracture types experience delayed healing with torsional instability. When simulating healing with clinically relevant torsional loading and fixator mechanics, published strain-based rules for tissue destruction predicted nonunions that would not be expected clinically. This suggested that clinical fracture healing may be more robust to distortional strain than has been

previously reported and that fuzzy logic models may require parameter tuning to correctly capture clinically relevant healing. Ultimately, this study is the first-ever model to include both fracture morphology effects and realistic implant mechanics and the proposed improved methods have the potential to extend into clinical fracture healing prediction.

1. Introduction

Through the process of tissue differentiation, bone heal by producing new tissues that eventually become indistinguishable from the original ones in the preinjury state, which is ascribed to be one of the unique properties of bone fracture healing [1], [2]. After a fracture, a broken bone usually repairs itself by a process known as *secondary healing*, in which a cartilaginous soft tissue structure called a *callus* will grow around the fracture line, progressively stiffen as it ossifies, and eventually remodel itself. Self-regulation of tissue differentiation is vital in the recovery [3], but is difficult to monitor continuously *in vivo*. Despite these challenges, animal and clinical studies have consistently shown that callus development is a mechanoregulated process that can be accelerated or disrupted by the local strain environment at the fracture site. If the interfragmentary mechanics are unfavorable, the healing process may be delayed. If delayed healing shows no evidence of radiographic progress for an extended period, it will be diagnosed as a *nonunion* [4]. Nonunion treatment is associated with an extended period of disability and multiple expensive and painful interventions to promote union [5]–[7]. In extreme cases, a false joint or pseudo-arthrosis may be generated [2].

In a clinical setting, progressive fracture healing is difficult to measure quantitatively. A wide range of risk factors may contribute to delayed healing or nonunion. Injury-related factors like excessive fracture gap, fracture classification [8]; Patient-dependent such as age [9], compartment syndrome , chronic disease, smoking [10]; Surgeon-dependent like impropriate implant, well-controlled trials are complex

to design. Large amounts of animal models have been used to show how the fixation mechanics influence the healing outcome. Especially, angular instability and shear disrupt bone formation. Recent research shows that fixation that allows excessive torsional rotation and shear movement significantly delayed the healing of diaphyseal osteotomies[11]–[14]. However, the osteotomy fractures in these models do not reflect the complex and diverse morphologies of clinical fractures, which are categorized by the OTA/AO Classification System [15](Figure 1).

One potential approach to bridge the gap between clinical observations, which are abundantly complex but lacking in end-point detail, and animal models, which are much more controlled and rich in detailed outcomes measures (e.g. computed tomography scanning, histology, and mechanical testing), is computational simulation of bone healing. The prevailing simulation techniques are based on the fundamental observation that new tissue formation is correlated with the local mechanical stimuli [16]. Since these relationships were first observed, many researchers have proposed theories to model strain regulation of three major processes: endochondral ossification, intramembranous ossification, and tissue destruction if the mechanical stimuli are unfavorable. In those models, numerical methods with fuzzy logic rules for mechanoregulation have been successfully implemented to simulate the bone healing response [17] and have been used to explore the utility of various definitions for the

mechanical stimuli that may influence the fracture healing process, such as principal

strain, deviatoric strain, and pore pressure [16], [18].
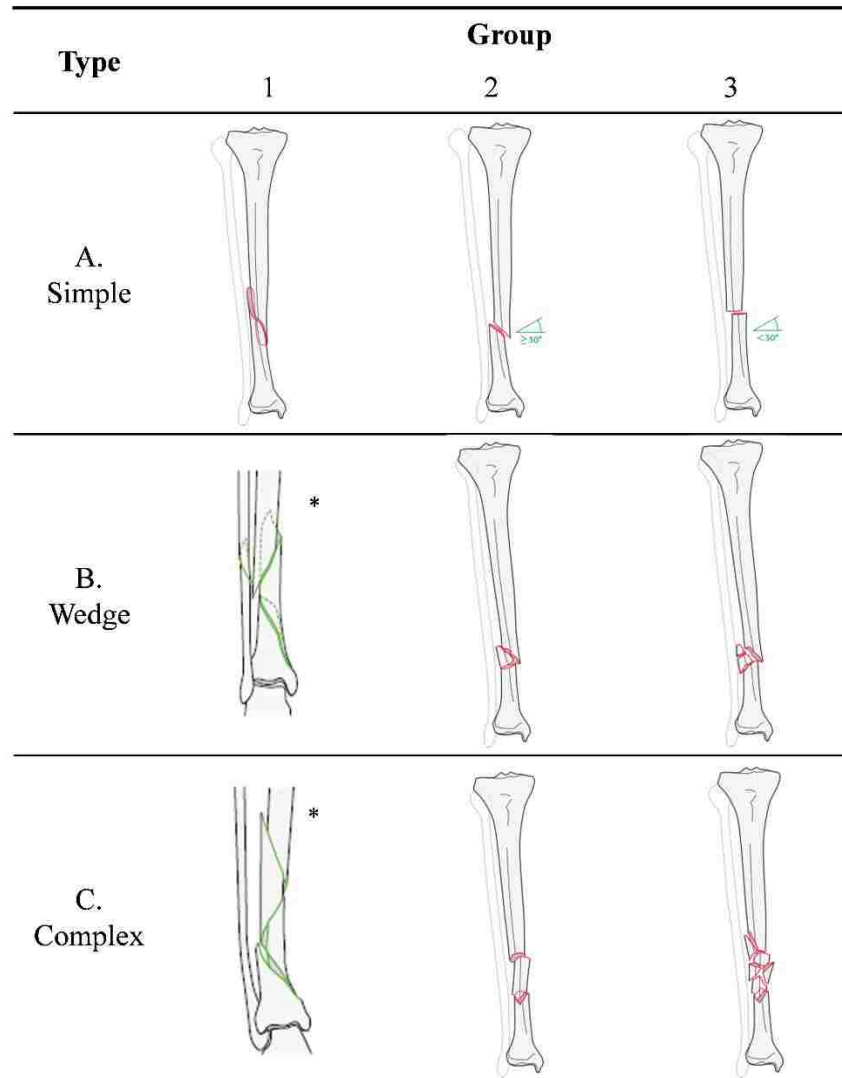
Figure 1: The morphology of the tibia diaphyseal segment fracture is defined as three categories from AO/OTA Classification. A1 – Spiral, A2 – Oblique, A3 – Transverse; B1 – Spiral Wedge, B2 – Spiral Wedge, B3 – Fragmented Wedge; C1 – Complex spiral, C2 – Segment, C3 – Irregular (B1 and B2 are excluded from the new 2018 Classification).

One common approach, and the method selected for this investigation, uses two

major mechanical stimuli: one for volumetric deformation, another for the local change

of shape [19]. This method was first validated in the literature by comparison to an

ovine transverse osteotomy fracture model and was shown to have the ability to predict

5

the bone healing under a single axial loading situation [20]. Other researches extended the technique to include the vascularity as another important factor in the tissue differentiation process, showing that new bone forms only if the blood perfusion is adequate [21]. In recent years, studies of healing outcomes in numerical simulation models under different loading conditions and fixation stiffness were performed and used to show that for simple transverse osteotomies, optimization of fracture treatment outcome can be accomplished by adjusting the fracture fixation stability [3], [22].

These results have generally supported preclinical and clinical observations that shear motion, particularly torsional instability, can disrupt healing. However, clinical fractures present with a wide variety of shapes of fracture bone. Previous numerical models have used only simple axisymmetric fracture geometries and 2D quadrilateral meshes to model fractures for comparison to animal studies. Those simplified models were not designed to replicate *in vivo* observations such as delays in healing with torsional instability or anticipated differences in healing rate between different fracture morphology types. Accordingly, the purpose of this work was to implement a fuzzy logic controlled mechanoregulation fracture healing simulation technique to explore the effect of clinically relevant fracture morphology on the interfragmentary mechanical environment, and in turn, on the speed of healing considering only strain-regulated mechanisms.

2. Methods

2.1 Geometries

The OTA/AO fracture classification, unified from Müller/AO and OTA systems, was designed to provide a standardized approach to the classification of long-bone fractures. Referencing this standard, we created idealized tibia diaphysis fracture models from nine geometry categories (OTA/AO 42-A/B/C types; see Figure 2) in SolidWorks 2018 (Dassault Systèmes SOLIDWORKS Corp., Waltham, Massachusetts, USA). In all models, the cortical shaft segments were axisymmetric with length, L = 50 mm, diameter, D = 17 mm, wall thickness, t = 3 mm, and volume, V = 7900 mm^3. These dimensions are consistent with previous idealized transverse osteotomy simulation models [22] , which were established for comparison and validation with respect to *in vivo* ovine fracture healing data. In all models, a consistent axial gap distance, d = 3 mm, was used to mimic accurate fracture reduction and normal healing conditions *in vivo* [16], [20].
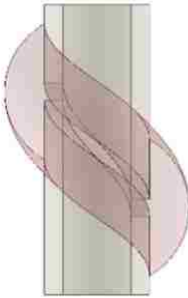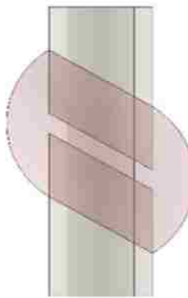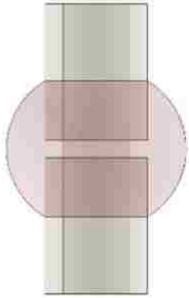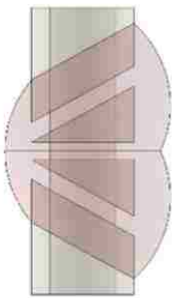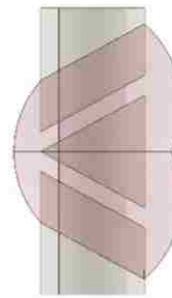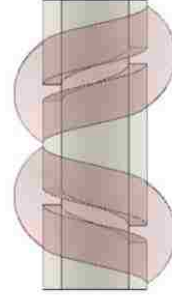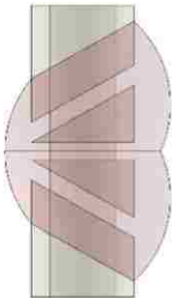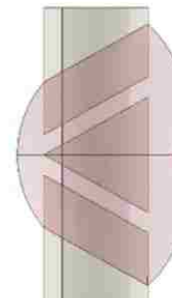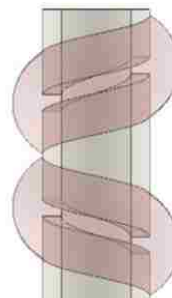
Figure 2: Idealized CAD models representing the AO/OTA classification of tibial fractures: A1 – Spiral, A2 – Oblique, A3 – Transverse, B1 – Spiral Wedge, B2 – Spiral Wedge, B3 – Fragmented Wedge, C1 – Complex spiral, C2 – Segmental, C3 – Irregular.
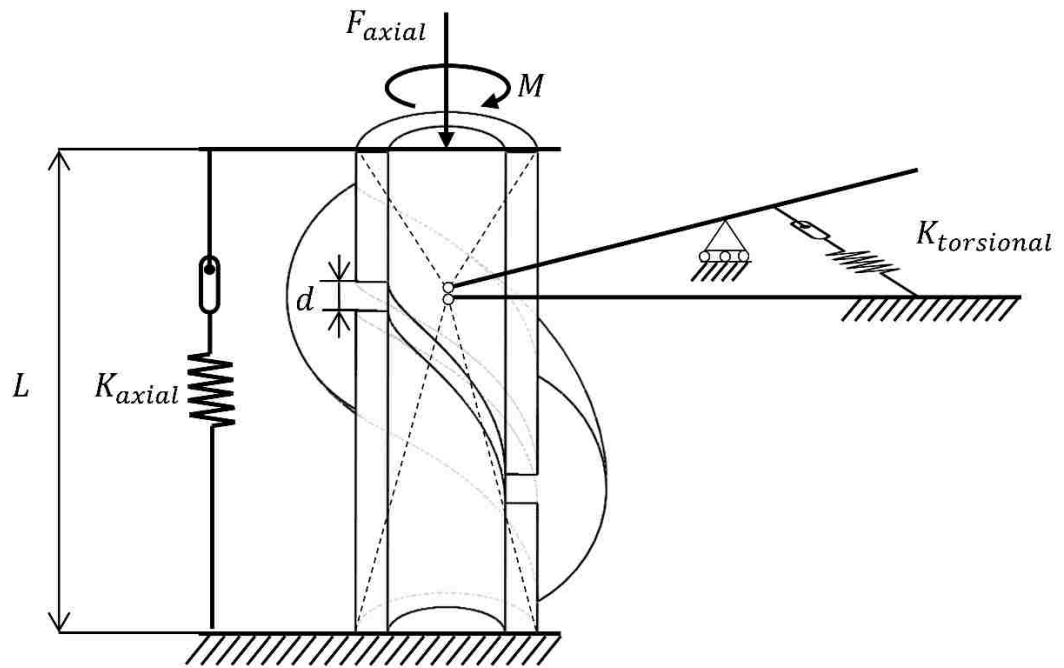
Figure 3: Model of spiral fracture callus geometry with the axial spring and torsional spring represents the IM nails. Loading Case I of an axial load only. Loading case II of an axial load and a moment.

2.2 Finite Element Models

All simulations were carried out in ANSYS 17.2 (Ansys, Inc., Canonsburg, PA, USA). The trabecular bone cylinder and the callus region were meshed with ten-node tetrahedral element (TET10). In the A1 model, the trabecular bone was meshed with 30030 elements while the callus region was meshed with 35098 elements. Max element size was set as 1.2mm to generate more than one layer of meshes between the gap region. The Boundary conditions of the FE models were supported in axial direction at the distal end of the cortical bone. The nodes at the axis of rotational symmetry were fixed radially.

An iterative simulation approach was used to predict the mechanoregulated healing response based on the strain conditions within the callus zone of each model, assuming an intramedullary (IM) nail was implanted. To define clinically relevant implant mechanics for the simulations, previously completed mechanical testing data for four commercial IM nailing systems (Biomet, Smith & Nephew, Stryker, and DePuySynthes) was reviewed [23]. Each implant system had been tested in axial and torsion loading in a multiaxial material testing machine.

In these tests, all of the commercial nailing systems allowed some free movement (see plateau in Figure 4), which arises due to the necessary dimensional clearance between the bone screws and the mating holes in the implant. This behavior occurs in both axial and torsion loading modes and is frequently misunderstood or misinterpreted because in most published papers, construct mechanics is generally

defined in terms of stiffness (e.g. axial stiffness [N/mm] or torsional stiffness [N-mm/deg]). Based on these tests, the mechanical behavior of IM nail in our models was modeled as a torsional spring allowing 8 degrees of free rotation followed by a linear torsional stiffness of 880 N-mm/deg (Figure 5a), and a nonlinear longitudinal spring allowing 0.2 mm of unrestricted axial compression followed by a linear axial stiffness 2650 N/mm (Figure 5b).
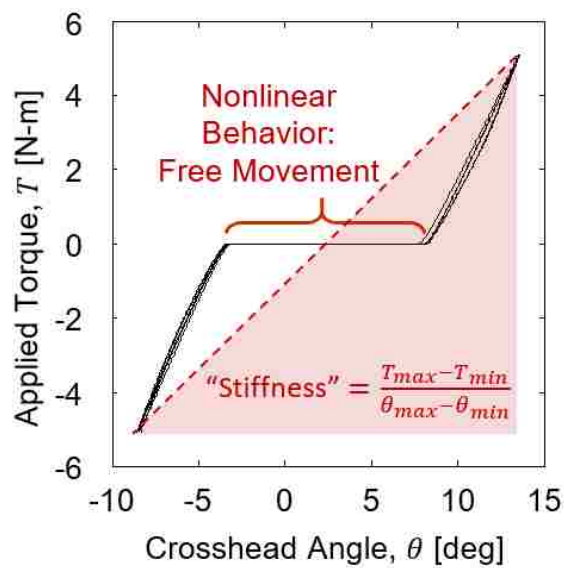
Figure 4: IM nail torsion bench test showing free movement occurring. Construct "stiffness" is frequently reported but misrepresents the nonlinear implant mechanics.

F

Applied Load [N]

$k_a = 2650 \ \dfrac{N}{mm}$

ΔF

Δd

Hysteresis
Loop Free
Movement

$\leftarrow 0.2 \rightarrow$

d

Axial Compression [mm]

(b)

M

Applied Torque [N-m]

$k_t = 0.88 \ \dfrac{N \cdot M}{dge}$

ΔM

$\Delta \phi$

Hysteresis
Loop Free
Rotation

$\leftarrow \quad 8 \quad \rightarrow$

ϕ

Angle of Twist [deg]
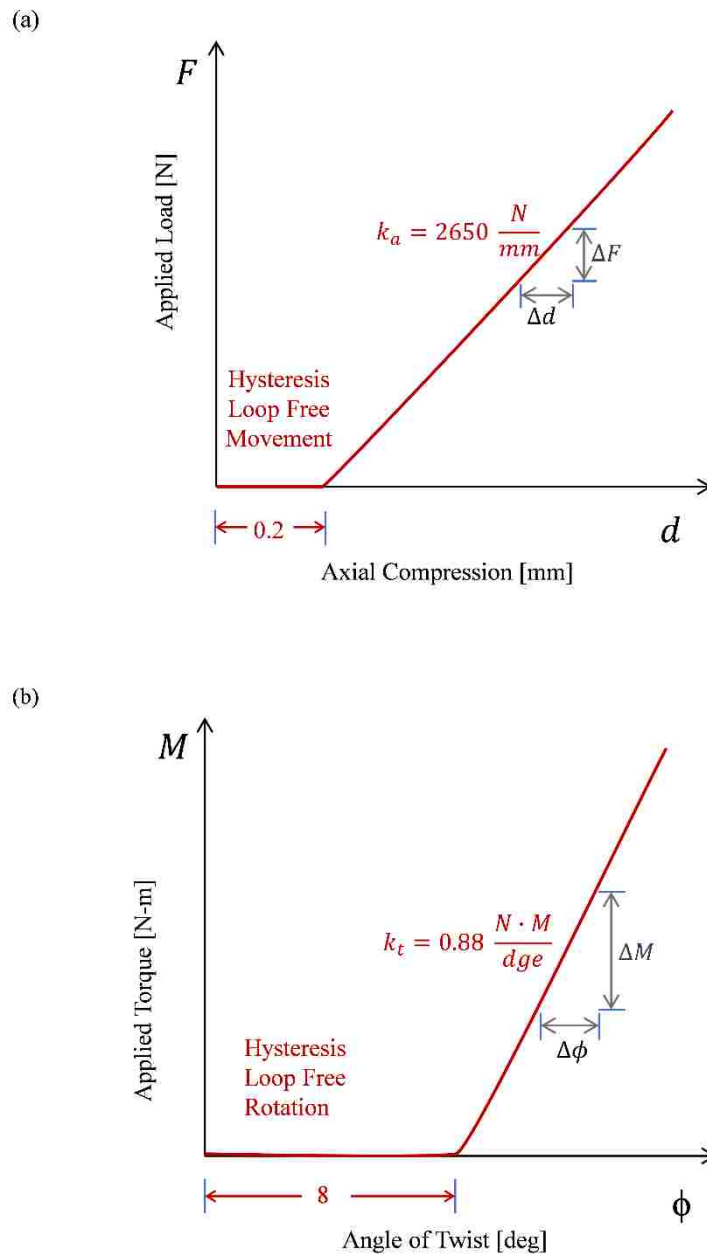
Figure 5. The mechanical behavior of a clinically relevant tibial IM nail construct was modeled using two nonlinear springs: (a) longitudinal spring; (b) torsional spring.

To simulate the forces that would be applied through the implant during the early stage of healing, conditions of partial weight-bearing (400 N axial load) were assumed. Previous investigators have frequently neglected torsional loading and

deformation in mechanoregulation models of bone healing [24], so these simulations were carried out under two loading conditions:

I. Partial weight-bearing (axial only): $400N$ axial compressive load, or about 50% of body weight for an average adult. This condition might be achieved when patients are instructed to begin immediate weight-bearing as tolerated (WBAT), which is generally considered safe for extra-articular fractures [25], [26].

II. Partial weight-bearing (axial + torsion): The same axial load from Case I above was applied in superposition with an additional 1 Nm torsional load. This torque is less than would be expected in normal full weight-bearing [27], but enough to ensure that both axial and torsional interfragmentary motion occur because the pure axial interfragmentary loading modes, such as simple axial compression or simple torsion, are not generally expected in clinical practice.

The fundamental premise of mechanoregulation simulations is that cell differentiation and tissue formation is directed by local mechanical strain. At any point, Cauchy's symmetric strain tensor can be written:

$$\varepsilon = \begin{bmatrix} \varepsilon_{xx} & \varepsilon_{xy} & \varepsilon_{xz} \\ \varepsilon_{21} & \varepsilon_{22} & \varepsilon_{23} \\ \varepsilon_{31} & \varepsilon_{32} & \varepsilon_{33} \end{bmatrix} = \begin{bmatrix} \dfrac{\partial u}{\partial x} & \dfrac{1}{2}(\dfrac{\partial u}{\partial y}+\dfrac{\partial v}{\partial x}) & \dfrac{1}{2}(\dfrac{\partial u}{\partial z}+\dfrac{\partial w}{\partial x}) \\ \dfrac{1}{2}(\dfrac{\partial u}{\partial y}+\dfrac{\partial v}{\partial x}) & \dfrac{\partial v}{\partial y} & \dfrac{1}{2}(\dfrac{\partial v}{\partial z}+\dfrac{\partial w}{\partial y}) \\ \dfrac{1}{2}(\dfrac{\partial u}{\partial z}+\dfrac{\partial w}{\partial x}) & \dfrac{1}{2}(\dfrac{\partial v}{\partial z}+\dfrac{\partial w}{\partial y}) & \dfrac{\partial w}{\partial z} \end{bmatrix} \quad (1)$$

The classical approach to bone healing simulation is to represent the mechanical stimulus by defining two scalar quantities from the general 3D state of strain – the dilatational strain, ε_{Hydro}, and the deviatoric strain, ε_{Dist}:

$$\varepsilon_{Hydro} = \frac{1}{3}(\varepsilon_{xx} + \varepsilon_{yy} + \varepsilon_{zz}) \tag{2}$$

$$\varepsilon_{Dist} = \frac{2}{3}\sqrt{(\varepsilon_{xx} - \varepsilon_{yy})^2 + (\varepsilon_{yy} - \varepsilon_{zz})^2 + (\varepsilon_{zz} - \varepsilon_{xx})^2 + 6*(\varepsilon_{xy} + \varepsilon_{yz} + \varepsilon_{zx})^2} \tag{3}$$

These strain components were obtained from ANSYS and the resultant mechanical stimuli (Hydrostatic and Distortional strains) for each callus element were extracted and calculated from ANSYS mechanical solutions using ANSYS Parametric Design Language (APDL).

2.3 Material Properties

In the finite element models, all materials were presumed linear elastic, isotropic, and homogeneous, with material properties for individual tissues defined in Table 1. Cortical bone fragments were assigned properties corresponding to intact bone and were kept constant throughout all iterations. Initially, all callus elements were assigned properties corresponding to granulation tissue. In the secondary bone healing process, connective tissues, cartilage, and woven bone are formed in the bridging callus at the fracture site over time. The local variation in the ratio of these three tissue types is determined by the tissue differentiation process, which in this model was assumed to be mechanoregulated. Accordingly, the degree of membership c was introduced to quantify the proportion of different tissue types of an element inside the callus region. The balanced equation of the degree of membership is given as:

$$c_{\text{woven}} + c_{cart} + c_{\text{conn}} = 1 \tag{4}$$

where c_{woven}, c_{cart}, c_{conn} denote the volume fraction of woven bone, cartilage, and connective tissues within the elemental tissue mixture, with the mechanical properties of all tissues given in Table 1. The degree of membership for each element within the callus region was defined with elementwise material properties.

Table 1: Tissue material properties used in simulations

Tissue Type	Young's Modulus, E_{FE} [MPa]	Poisson's Ratio, v_{FE} [-]
Intact bone	15,750	0.45
Woven bone	4,000	0.45
Cartilage	40	0.35
Connective tissue	0.5	0.3

Tissue differentiation as a continuous process occurs within the callus as the healing process proceeds. Consequently, the material properties of each callus element were updated in each iteration based on new volume fractions with a linear rule of mixtures, as has been previously reported [17]:

$$E_{FE} = E_{woven}c_{\text{woven}} + E_{cart}c_{cart} + E_{conn}c_{\text{conn}} \qquad (5)$$

$$v_{FE} = v_{woven}c_{\text{woven}} + v_{cart}c_{cart} + v_{conn}c_{\text{conn}} \qquad (6)$$

2.4 Fuzzy Logic Controller

The Fuzzy Logic Toolbox (ver. 2.3.1) in MATLAB R2017A (MathWorks, Inc., Natick, MA, USA) was used to characterize the process of tissue differentiation during the healing process. The fuzzy controller took in the output files of the strain results from the ANSYS simulation as fuzzy inputs, determined the input state for each element in the callus region based on fuzzy logic rules, and output which kind of biological process would happen to predict the tissue differentiation result (Figure 6).
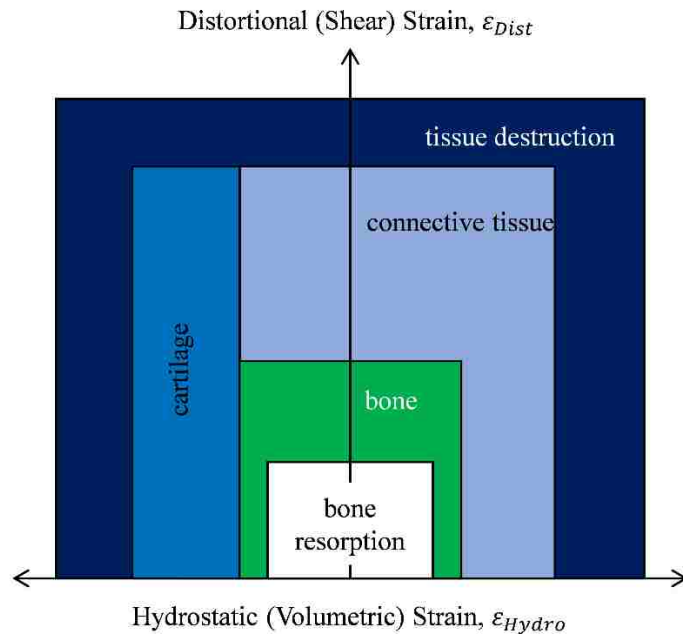
Figure 6: Tissue differentiation diagram based on previous research [28]. The boundaries between the regions are fuzzy zones rather than thresholds.

At the start of each iteration, the input state of each element was evaluated in the ANSYS finite element model as described above with elementwise material properties dictated by the tissue volumetric rules of mixtures (Equation 5 and Equation 6) at the previous iteration. The input variables to the fuzzy logic controller included the octahedral normal and shear scalars, ε_{Hydro} and ε_{Dist}, as well as the volume fractures for bone and cartilage, c_{bone} and c_{cart}.

$$Inputs = [\varepsilon_{Hydro} \quad \varepsilon_{Dist} \quad c_{Bone} \quad c_{Cartilage}] \tag{7}$$

Membership functions were used to regulate the degree to which the inputs belonged to each of the fuzzy sets. In the process of fuzzification, each of the fuzzy inputs was defined with its fuzzy sets consisting several membership functions (Table 2) which maps the non-fuzzy input values to fuzzy linguistic terms between 0 and 1. For example, for a given fuzzy input **A** (Distortional strain values) on the universe of discourse **X** (Distortional strain). The value **0** means that **X** is not a member of the fuzzy set; the value **1** means that **X** is fully a member of the fuzzy set. The values between **0** and **1** characterize fuzzy members, which belong to the fuzzy set only partially.

Table 2. Fuzzy inputs and associated membership functions

Fuzzy input	Fuzzy set	Membership functions
Distortional strain hydrostatic strain	'Very High', 'High', 'Middle',' Near Zero' 'Positive Very High', 'Positive High', 'Positive Middle', ' Near Zero', 'Negative Middle', 'Negative High', 'Negative Very High'	
Bone concentration	'High', 'Middle',' Low'	Trapezoidal
Cartilage concentration	'High', 'Middle',' Low'	

After the inputs were fuzzified, 24 linguistic *If-Then* rules were defined to control tissue differentiation during healing process (see Figure 7 and Table 3). For example, one rule for cartilage formation can be expressed linguistically:

IF % Cartilage (c_{cart}) is *Not Low* **AND** Normal Strain (ε_n) is *Negative High* **AND** Shear Strain (ε_s) is *Not Destructive* **THEN** increase % Cartilage (c_{cart}).

18
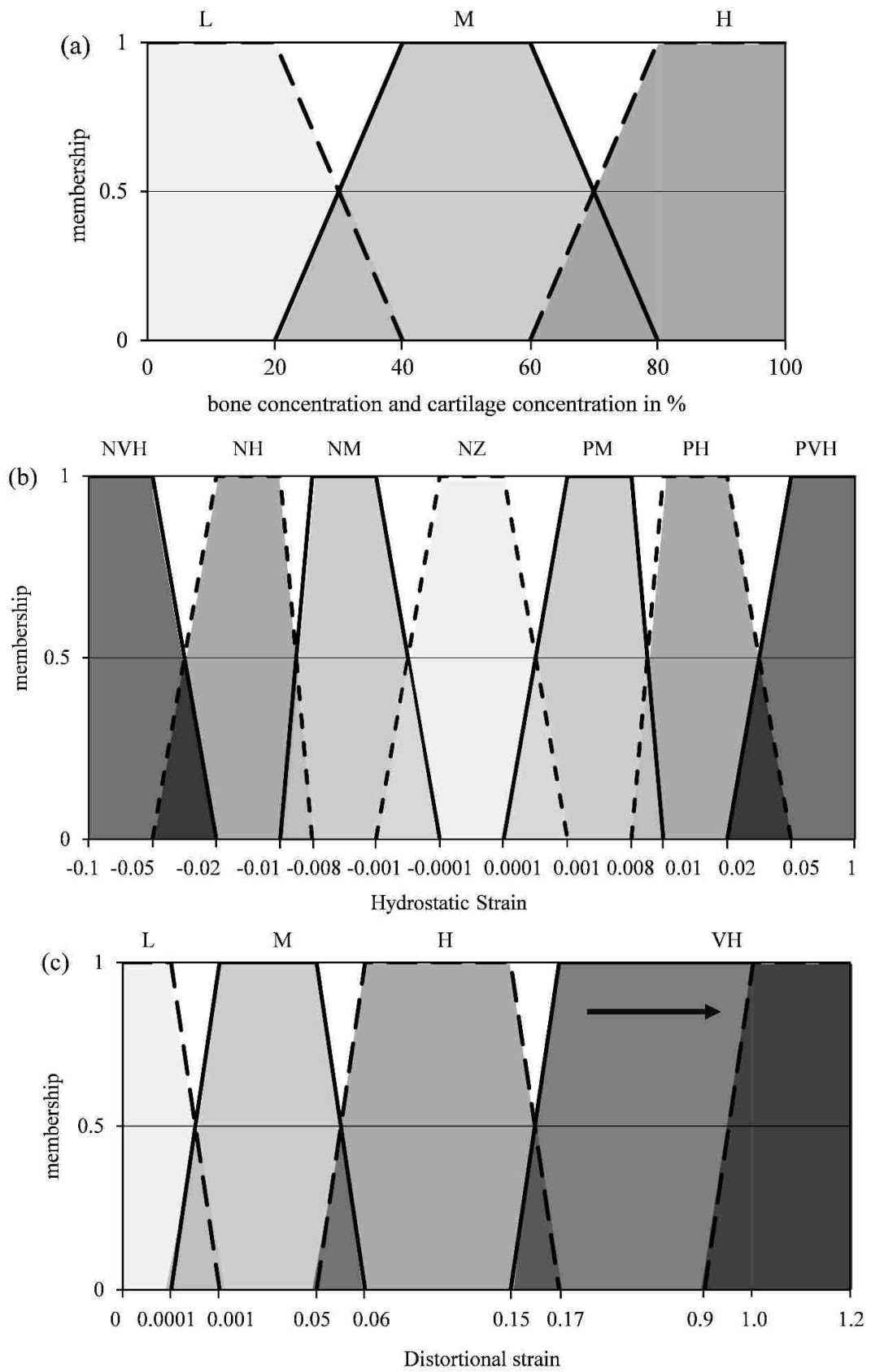
Figure 7: (a) Membership function of bone, cartilage concentration. (b) Membership function of hydrostatic strain. (c) Membership function of distortional strain.

Table 3: Fuzzy rules implemented in the fuzzy controller

Rules	Mean Strain	Shear Strain	Bone Volume Fraction, c_{woven}	Cartilage Volume Fraction, c_{cart}	Bone Change	Cartilage Change
1	Positive very High				Decrease	Decrease
2	Negative Very high				Decrease	Decrease
3		Very high			Decrease	Decrease
4	Low	Low			Decrease	Decrease
5	Negative medium	Medium		Low	Increase	Decrease
6	Positive medium	Medium		Low	Increase	Decrease
7	Low	Medium		Low	Increase	Decrease
8	Negative medium	Not very high	Not high	Low	No change	increase
9	Negative high	Very high		Not low	No change	Increase
10	Negative medium	Very high		High	No change	Increase
11	Negative medium	Low		Not low	Increase	decrease
12	Negative high	Low		Not low	Increase	Decrease
13	Negative medium	medium		Not low	Increase	Decrease
14	Negative medium	Medium		Not low	Increase	Decrease
15	Negative medium	Medium	High	Low	Increase	Decrease
16	Negative medium	Low	High	Low	increase	Decrease
17	Negative medium	High			No change	No change
18	Low	High			No change	No change
19	Positive medium	High			No change	No change
20	Positive medium	Not very high			No change	No change
21	Negative high	Not very high		Not low	Increase	Decrease
22	Negative medium	Not very high		Not low	Increase	Decrease
23	Low	Not very high		Not low	Increase	Decrease
24	Positive medium	Not very high		Not low	Increase	Decrease

Finally, defuzzification was performed according to the membership function of the output variables describing the process of interpreting the membership degrees of the fuzzy sets into a specific decision or real value. The resulting end state probabilities included the likelihood tissue destruction (p_{TD}), intramembranous ossification (p_{IO}), cartilage formation (p_{CF}), endochondral ossification (p_{EO}), cartilage calcification (p_{CC}), remodeling (p_R), and no change (p_{NC}). In vector form, the differentiation probabilities are:

$$\boldsymbol{p} = [p_{IO} \quad p_{CF} \quad p_{EO} \quad p_R \quad p_{NC} \quad p_{CC} \quad p_{TD}] \tag{8}$$

To illustrate how the fuzzification, linguistic rule application, and defuzzification processes work, consider this example of an arbitrary finite element inside the callus region. Suppose the mechanical stimuli are ε_n = -0.0001 and ε_s = 0.057 and the tissue volume fractions are c_{woven} = 2% and c_{cart} = 10%. This elemental input condition fits fuzzy rules 6 and 7 (see Table 2) which means both rules will be activated. Multiple rules have been activated because there are several overlapping regions in which the input condition fall in the membership function. In this example, the tissue differentiation result has the probability of 30% to be "Intramembranous Ossification", 70% to be "No Change", and 0% to be all the other outputs.

After the differentiation probabilities for each element have been calculated, the concentration of woven bone and cartilage for the next time steps then can be calculated:

$$c_{\text{woven},t+1} = c_{\text{woven},t} +$$

$$c_{\text{woven},t} \begin{bmatrix} p_{TD} & p_{IO} & 0 & p_{EO} & p_R & 0 & p_{CC} \end{bmatrix} \begin{bmatrix} -R_{TDB} \\ R_{IO} \\ 0 \\ R_{EO} \\ -R_{RB} \\ 0 \\ R_{CC} \end{bmatrix} \Delta t \qquad (9)$$

$$c_{\text{cart},t+1} = c_{\text{cart},t} +$$

$$c_{\text{cart},t} \begin{bmatrix} p_{TD} & 0 & p_{CF} & p_{EO} & p_R & 0 & p_{CC} \end{bmatrix} \begin{bmatrix} -R_{TDC} \\ 0 \\ R_{CF} \\ -R_{EO} \\ -R_{RC} \\ 0 \\ -R_{CC} \end{bmatrix} \Delta t \qquad (10)$$

Where the rate constants $R_{TDB}, R_{TDC}, R_{IO}, R_{CF}, R_{EO}, R_R, R_{RC}, R_{CC}$ represent the following biological processes: tissue destruction of bone (R_{TDB}), tissue destruction of cartilage (R_{TDC}), intramembranous ossification (R_{IO}), cartilage formation (R_{CF}), endochondral ossification (R_{EO}), remodeling of bone (R_{RB}), remodeling of cartilage (R_{RC}), and cartilage calcification (R_{CC}). The parameter values chosen for each of these rate constants can be found in Table 3. Δt means the time interval between each iteration, in our model, was set to be 1 day. The new material properties can be calculated by the rules of mixture.

Note that blood supply is a very important factor for the osseous healing [29]. While the chondrogenesis and the calcification of the fibrocartilage may precede the angiogenesis, intramembranous and endochondral ossification rely entirely on sufficient perfusion. Cartilage forms instead of woven bone if mechanical stimuli are

inadequately large or local blood perfusion is too low for intramembranous ossification [21]. This model assumed a permanent homogeneous optimal blood supply for all elements inside the callus region with no linguistic rules for perfusion-limited differentiation. These could be easily added but were not varied in this body of work.

Table 4: Tissue transformation rates of fuzzy rule conclusions [17].

Fuzzy conclusion	From	To	Rate [%/day]
Tissue Destruction of bone	Bone	Conn. tissue	10
Tissue Destruction of cartilage	Cartilage	Conn. tissue	20
Intramembranous ossification	Conn. tissue	Bone	1
Cartilage formation	Conn. tissue	Cartilage	5
Endochondral ossification	Cartilage	Bone	2
Remodeling of bone	Bone	Conn. tissue	4
Remodeling of cartilage	Cartilage	Conn. tissue	8
Cartilage calcification	Cartilage	Bone	2
No change			

2.6 Healing Assessment over Time

A widely applied method is accomplished by measuring the biomechanical properties of skeletal tissues to assess the recovery condition. The ideal status of bone recovery is not considered achieved when the mechanical performance of the newly developed tissues at the fracture site is not restored [30].

As healing progresses, the granulation tissue of the initial callus will be gradually replaced with a mixture of stiffer tissues, leading to a progressive stiffening of the entire callus region and decreased interfragmentary motion and strain [16]. To measure the healing status at the fracture site, a virtual torsion rigidity (VTR) test was chosen as a summary indicator of mechanical integrity. Post-mortem torsion testing is commonly used to determine the extent of recovery in animal models [11], [14], [31], because the results produced are direction-independent, unlike bending tests [32]. In the models, torsion mechanical testing was carried out at each iteration in a correspondent testing model that had the same settings as in each simulation model while excluding the intramedullary nail, just as would be the case in post-mortem mechanical testing in an animal model. This ensured that the mechanical result measured the structure of the callus only, not the implant. Torsion tests consisted of an applied one degree of rotation at the proximal end of the bone and calculation of the resulting reaction moment at the fixed end. Torsional rigidity across the fracture site, R_{tor} was assessed at the end of each step:

$$R_{tor} = \frac{ML}{\phi} \tag{11}$$

Where M is the reaction moment, L is the segment length, and ϕ is the angle of the twist. Healing progress over time was measured by normalizing the torsional rigidity of the fractured model to the torsional rigidity of a comparison model consistent of intact cortical bone with no defect. Iterations were repeated for 100 steps in each model to estimate the patient's healing status within 100 days after the surgery.

2.7 Iterative Healing Simulation Procedure

In the model, tissue differentiation occurs continuously within the callus as the healing process proceeds (see Figure 6). First all elements of the callus were initialized to connective tissue. Each iteration involved application of loading (Case I or Case II, see §2.2 for rationale). At the beginning of each iteration, the strain status of each elements was measured in ANSYS; the degree of membership and tissue differentiation results were estimated using fuzzy logic controller; and the degree of bone formation was examined, then the rule of mixtures (Equation 6 and Equation 7) was then used to update E and ν for each mesh element. After each iteration,. The strain status of all callus elements was updated and used to determine the tissue mixture change for the next iteration using the fuzzy controller described above. Finally, at each step, the structural progress of healing was measured using a virtual torsion test as described in §2.6. Thus, the healing process in our numerical method was modeled by iterations (see Figure 8).

In the simulation models, each iteration was used to represent the approximate daily healing process, as had been done by previous investigators [17].
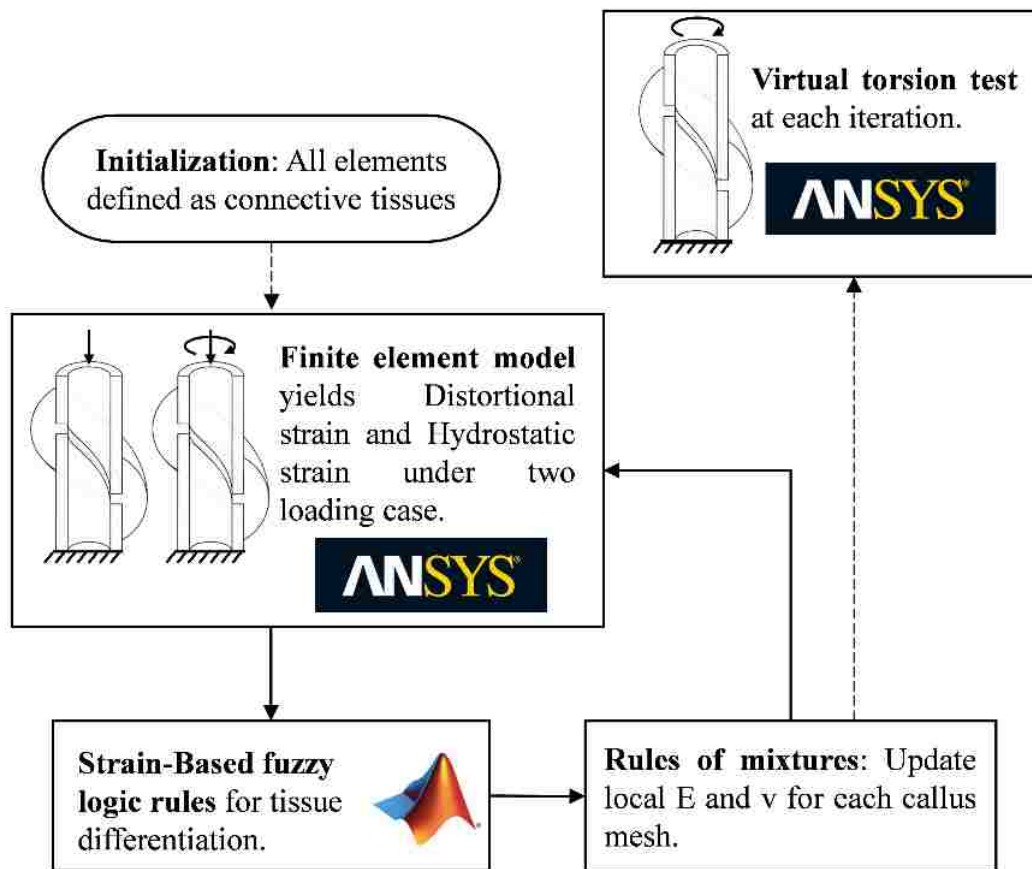
Figure 8: Flowchart of the fracture healing model including the FE method and the fuzzy logic.

3. Results

In general, as in all computational mechanoregulation models of fracture healing, these models predicted formation of cartilage and bone, with progressive stiffening of the callus over time (see representative example in Figure 9).
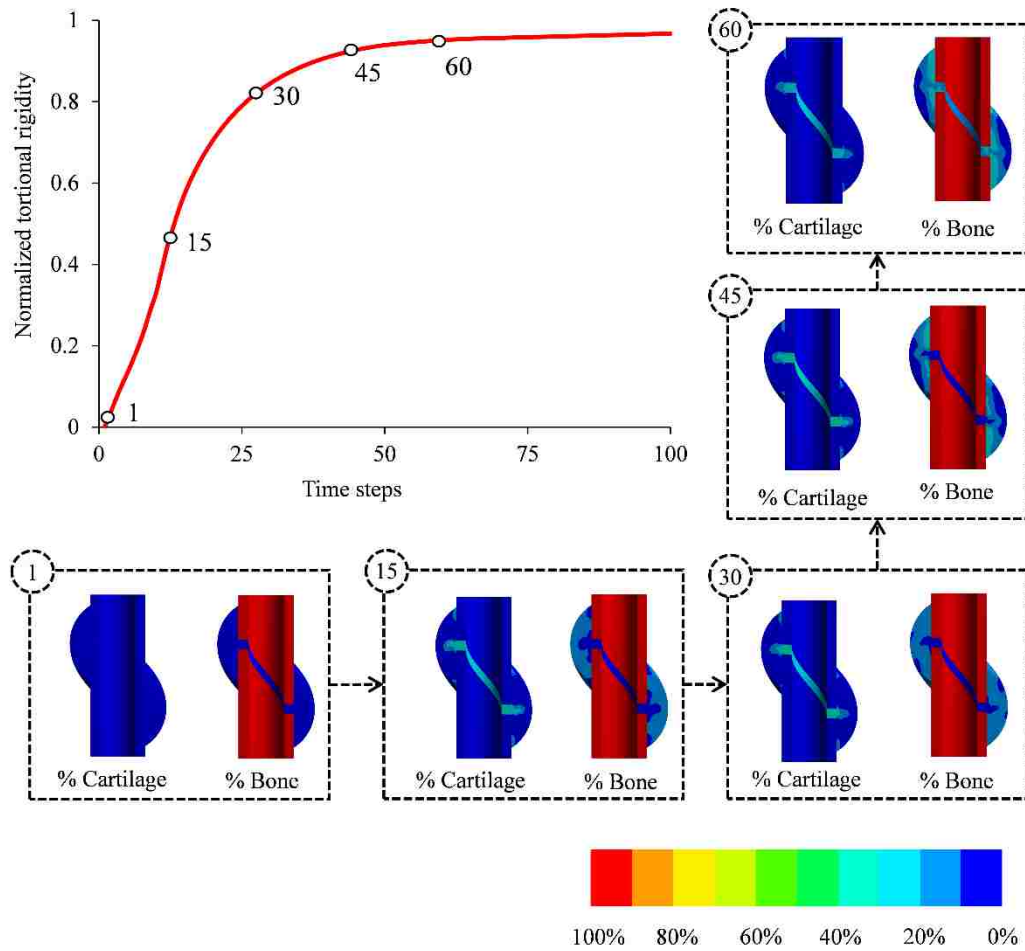
Figure 9: Prediction of bone and cartilage concentration for A1 geometry under loading case I.
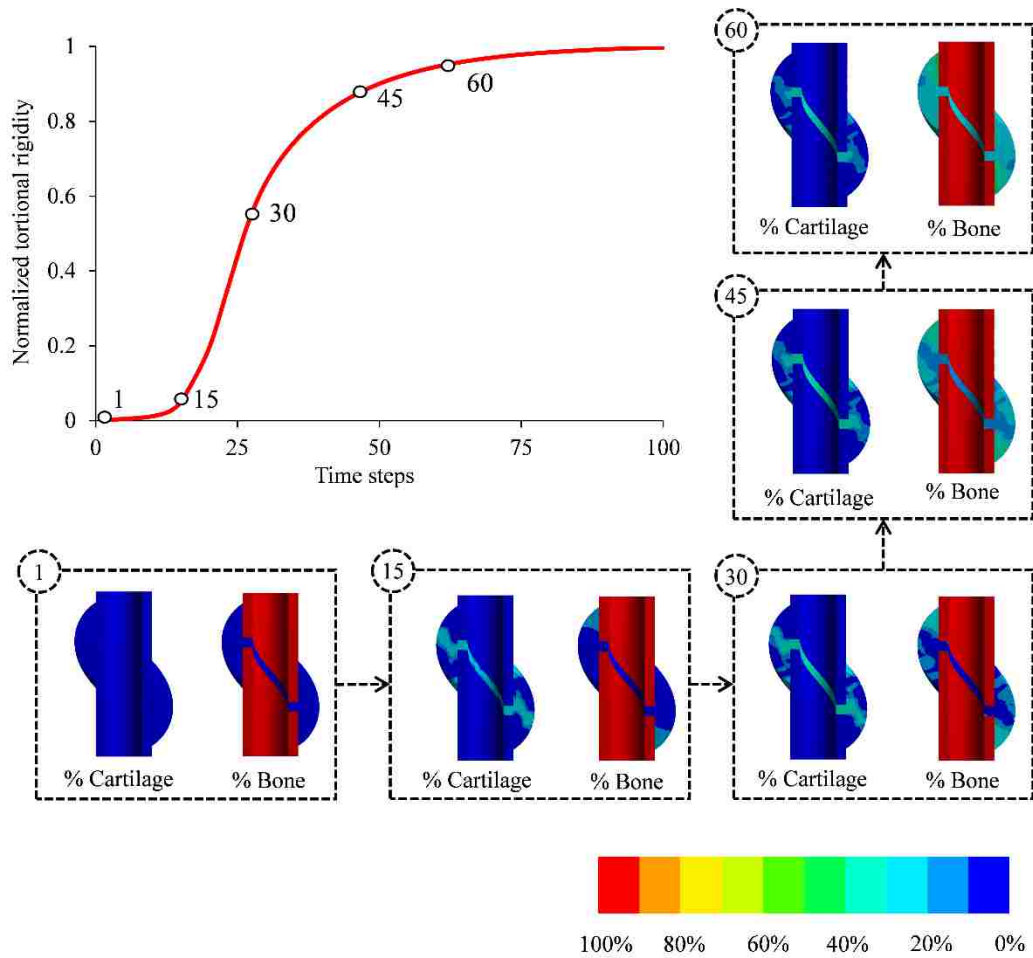
Figure 10: Prediction of bone and cartilage concentration for A1 geometry under loading case II.

Recorded variables at each iteration included the predicted distributions of all input variables (strains, element stiffness, and tissue concentrations) inside the callus region. As described in Figure 8, the torsional rigidity, R_{tor}, of the bone-callus structure was assessed at each iteration and was normalized to the rigidity of the intact bone to provide a relative measure of healing over time on a percentage scale. This procedure was repeated for all nine OTA/AO geometries under both loading cases I and II for 100 iteration days. In all models, when R_{tor} approached 100%, this represented

standard uncomplicated healing of the fractured bone. If R_{tor} remained substantially low over the 100 iteration days, this was considered a model-predicted nonunion.

First, we attempted to compare the two loading scenarios (I – axial only; II – axial and torsion) for the three simplest geometry models in the data, which represent OTA/AO classifications A1 (simple spiral), A2 (simple oblique), and A3 (simple transverse). When simulated for 100 days, progressive healing occurred as expected in for the axial-only loading scenario (Figure 10a), but did not occur when clinically relevant torsional instability was introduced into the simulated implant construct (Figure 10b). In fact, less than about 1% recovery was observed for these three fractures under the loading case II over the 100 iterations, compared with at least 90% recovery for the axial-only loading Case I. This result was surprising because in clinical practice, nonunions are rare for these simple fractures, particularly when there is good vascularity (optimal perfusion in this model).
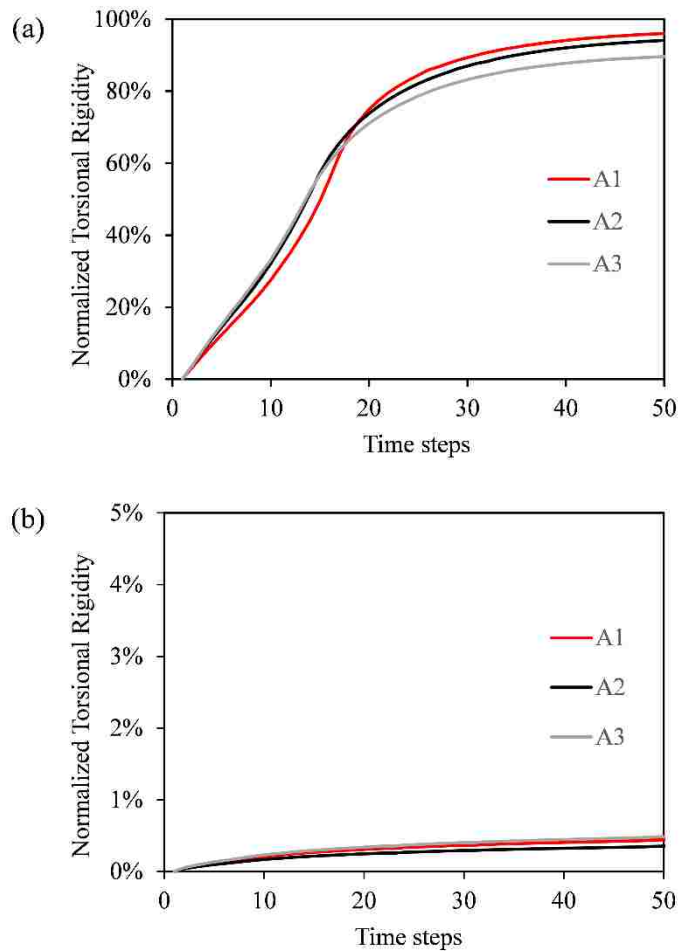
Figure 11: Progression of bone-callus normalized torsional rigidity during the early healing period of the A1, A2 and A3 model in the two loading cases: (a) Case I – axial loading only; (b) Case II – axial and torsion loading.

A closer examination of the data produced with the published mechanoregulation models under the torsional loading case provided a mechanical strain explanation for the predicted slow healing. When the implant model was configured to allow realistic torsional instability, the resulting callus strain field included large regions of high distortional strain from the first iteration (see Figure 11). According to the published mechanoregulation rules, under these scenarios, fracture callus will fail to achieve bony bridging because the elements inside the callus region experience extremely high distortional strain conditions that have been previously

31

attributed to tissue destruction conditions. According to the published mechanoregulation rules, the tissue in the navy-blue region of Figure 11 were destructed, exceeding the supposed limit for formation of woven bone. As a result of these distortional strains, this model set predicted no bony bridging between the distal and proximal fragments. Most of the tissue in the grey region were in the phase of intra-membranous ossification (cortical bone are not included); the tissue in the green and sky-blue region were in the process of endochondral ossification.
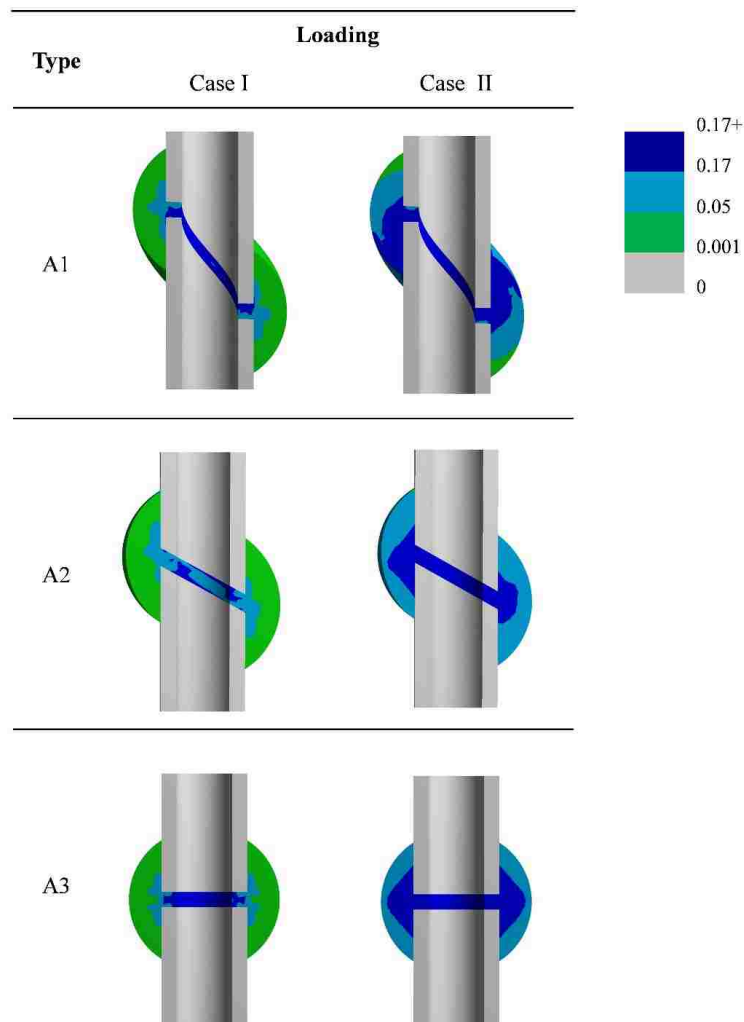
Figure 12: Distortional strain results for A1, A2 and A3 model in both loading at the first iteration. Note the large regions of destructive strain according to published baseline fuzzy logic mechanoregulation models.

32

Based on the results for Cases I and II in OTA/AO fractures A1, A2, and A3, the traditional fuzzy rules for distortional shear destructive cutoff worked well when modeling fracture healing under axial loading only, but failed to produce union when predicting healing outcomes under multiaxial loadings. The elemental strain distributions within the callus zone for the first iteration are illustrated in Figure 12.
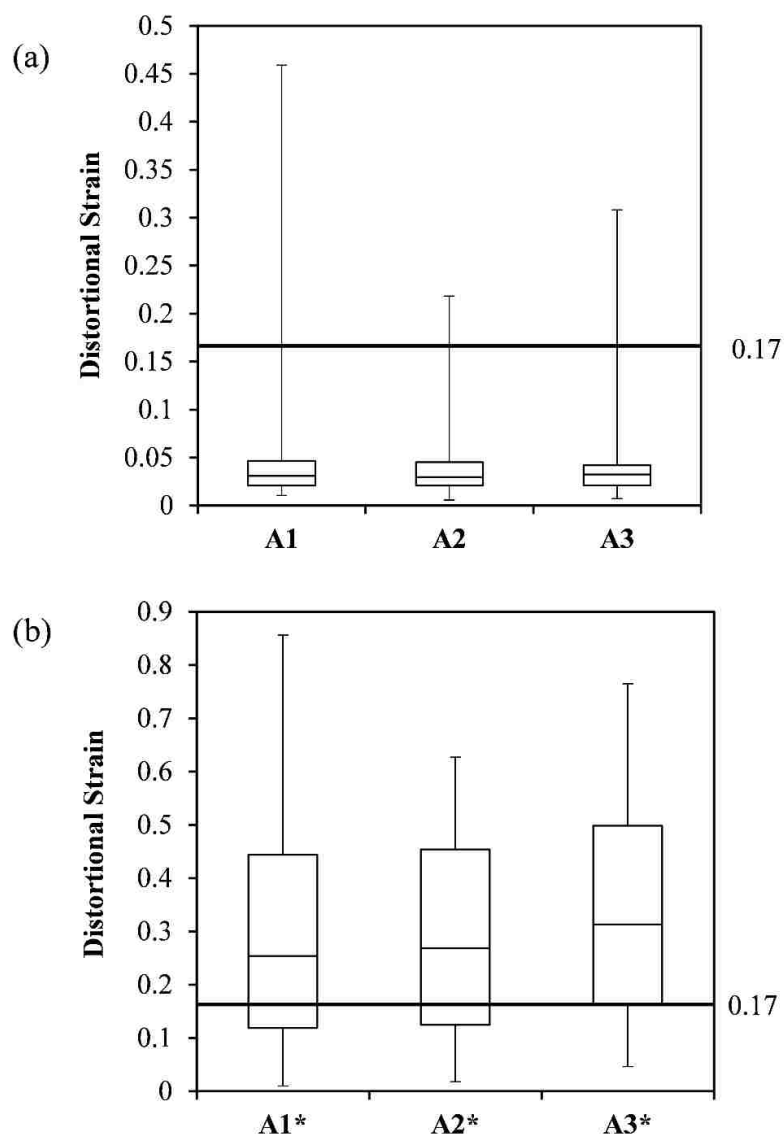
Figure 13: Box plot of elemental distortional strains in A1, A2, A3 geometries at the first iteration. A1 represents the strain distribution at loading case I, while A1* represents the strain distribution at loading case II, et al. The dash line shows the upper tissue formation limit.

Figure 12 shows that most of the elements fell into the region that would be favorable for tissue destruction at loading condition case II, resulting in the healing curves shown in Figure 10(b), even though this would not be expected clinically. To address this issue, the tissue destruction cutoff for distortional strain was increased from the previously published cutoff of 0.17 to an unrestrictive upper limit approaching 1.0. This limit was not chosen based on an expected physiological mechanism, but rather to avoid producing tissue destruction in the fuzzy model. This adapted model was then run for 100 iteration days, producing the healing curves shown in Figure 13.

Figure 14: Progression of callus torsional rigidity during the early healing period based on fracture geometry, grouped by OTA/AO type. A1 means at loading case I while A1* means at loading case II, et al.
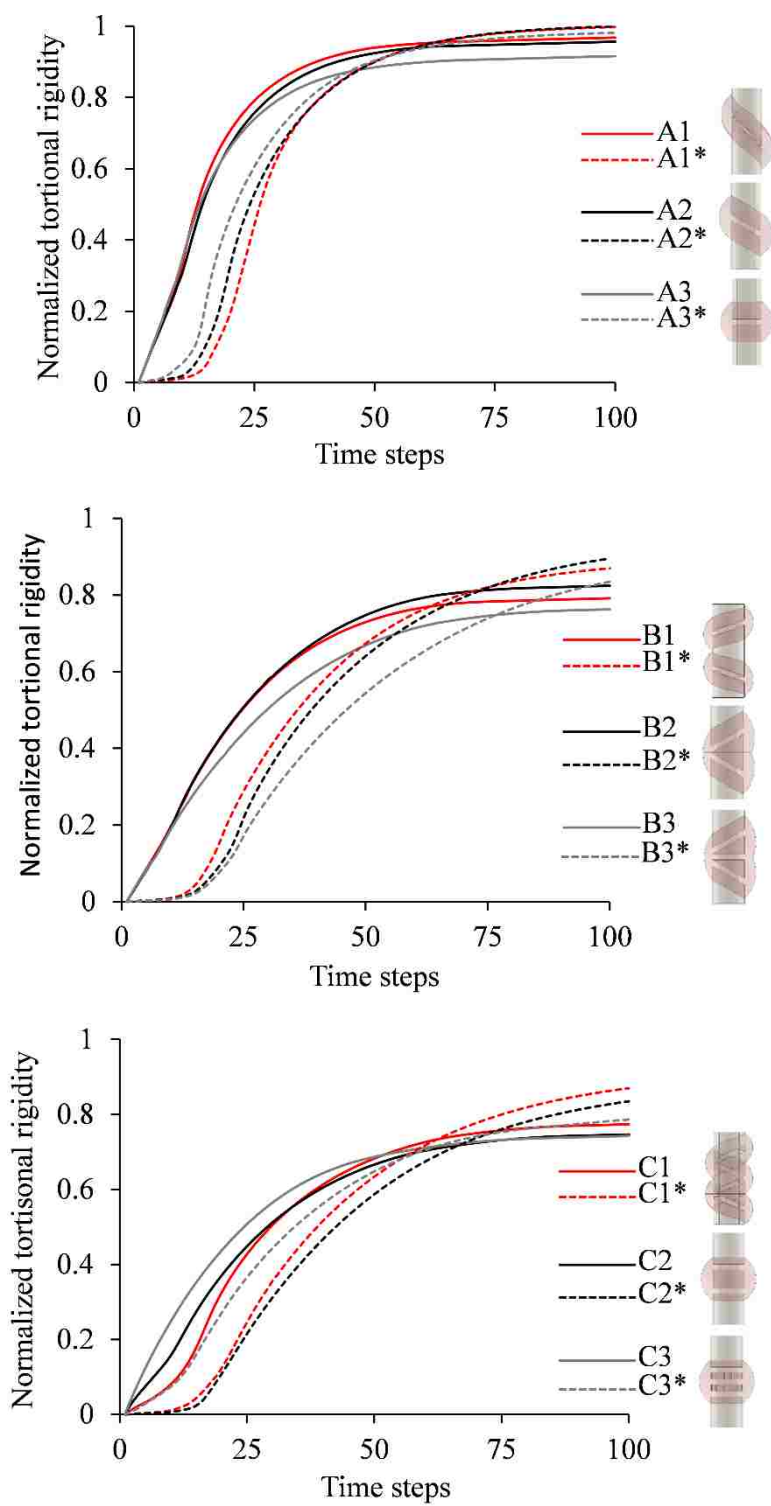
After effectively removing the distortional strain-mediated destruction term from the fuzzy model, the new simulations showed that progressive healing would occur across all fracture types, even with torsional loading and realistic implant mechanics (Case II). Across all nine fracture models, the simulations showed that torsional instability, which occurs naturally in realistic intramedullary fixation, can delay healing slightly compared to perfect torsional rigidity. The progression of callus torsional rigidity showed a plateau at the early period of healing for all the nine models in the loading case II compared to the loading case I. This delay was around 15 days for type B and C fractures compared to one week for type A fractures. After this initial delay, healing began to progress rapidly and the bone-callus torsional rigidity then increased at approximately the same rate as in the perfect torsional stability scenario, just at a later absolute time point.

The model results also indicated that differences in interfragmentary strain due to fracture geometry can significantly change the time to union. Overall, OTA/AO type B (wedge) and C (complex) fractures healed more slowly than type A (simple) fractures, even when all fuzzy logic parameters were kept constant in both loading cases. After 100 iteration days (~3 months), all simple (A) fractures were approaching $R_{tor} = 100\%$, whereas the wedge (B) and complex (C) fracture models, all of which had at least one floating bone fragment, were at 80% or less recovery according to Figure 13.

Besides virtual torsional rigidity test (Figure 13), overall healing simulation results of nine geometry were indicated by measuring Young's Modulus (Figure 14) and volume fraction of different tissue types (Figure 15) in the fracture site at the 100th iteration (final healing statue).

Figure 14 shows that the Young's Modulus of the fracture under loading case II were to some extent greater than the one under loading case I. This is not surprising that multiaxial loading would stimulate more area within the callus region to recover, which in turn leads to a slightly better mechanical performance in the virtual rigidity test at later stage shown in Figure 13.
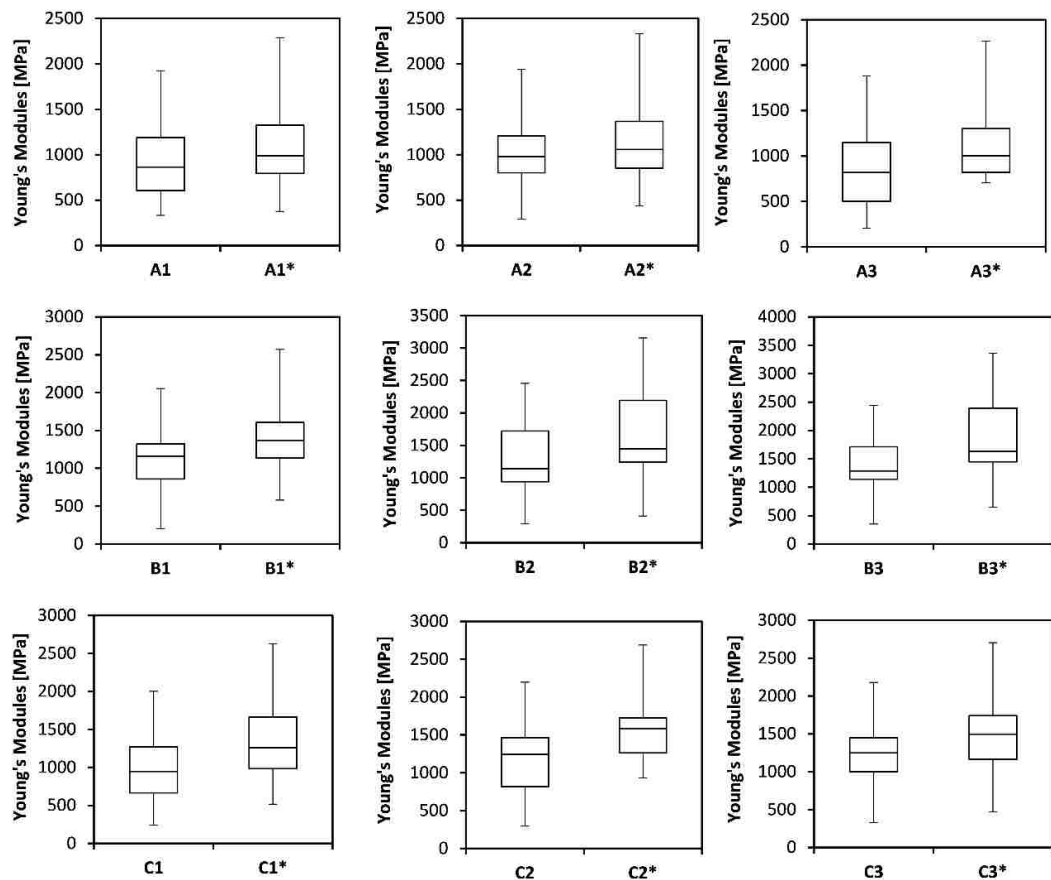
Figure 15: Distribution of elemental Young's modulus for all 9 geometries at 100 times of iteration.

Figure 15 shows the volume fraction of woven bone, cartilage and connective tissue for all 9 geometries under two loading case during the iterations. Even when the volume fraction of bone did not reached 100%, the bone had already processed with the similar mechanical properties to resist loading moment resembling patients' daily bearing. Figure 15 also validates the conclusion from Figure 13 that the healing was delayed under the loading case II for all geometries. The progression of volume fraction of woven bone (red dash line in Figure 15) showed a plateau at the early period of healing for all nine models under the loading case II which means the tissue went through the Endochondral Ossification instead of Intramembranous Ossification. Notably, more cartilage tissues would produce under loading case II than under loading case 1.
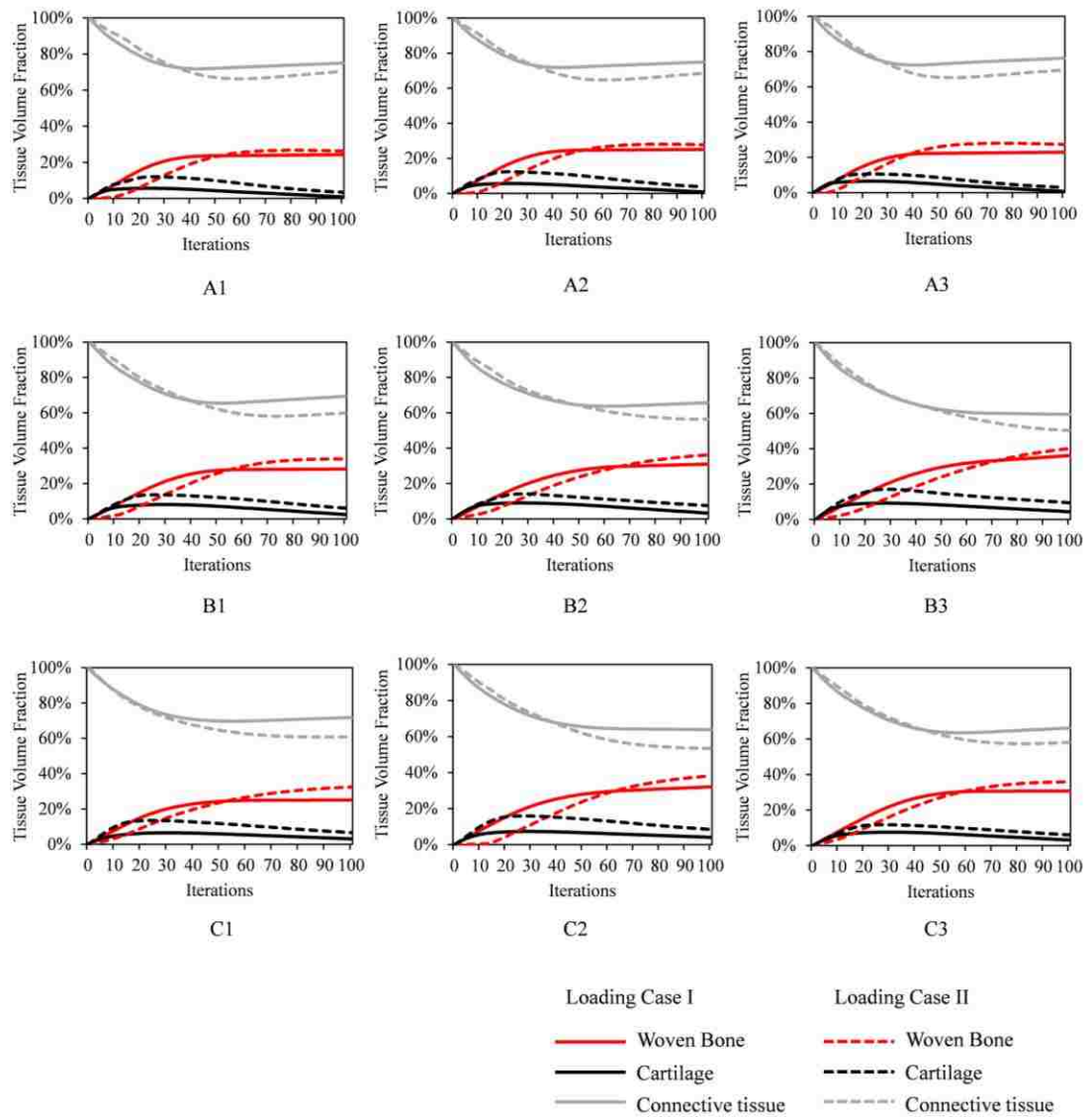
Figure 16: Progression of volume fraction of woven bone, cartilage, and connective tissue for all 9 geometries under two loading case during the early healing period.

The models were meshed with Tet10 elements. To verify that the FE model predictions were independent of the FE mesh size, a mesh convergence analysis was performed. Three different sizes of max face size factors were set (2.4 mm, 1.2 mm, 0.6 mm) to find a suitable mesh size corresponding to the gap between cortical bone (Figure 16).
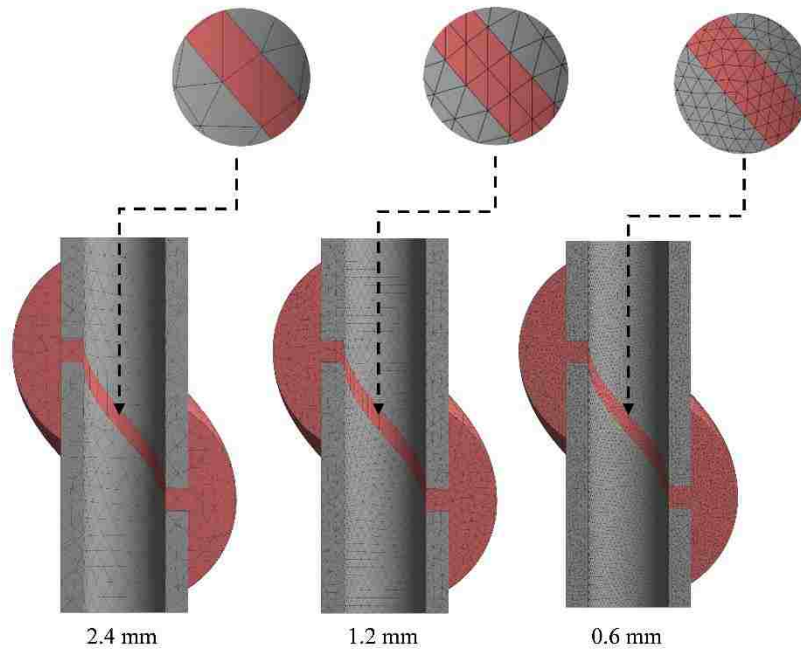
Figure 17: Three different mesh sizes which depends on the layer of mesh that generated at the gap region of the cortical bone for model A1.

The axial loading was applied to these three different mesh sizes and the Progression of callus torsional rigidity curves are shown in Figure 17.
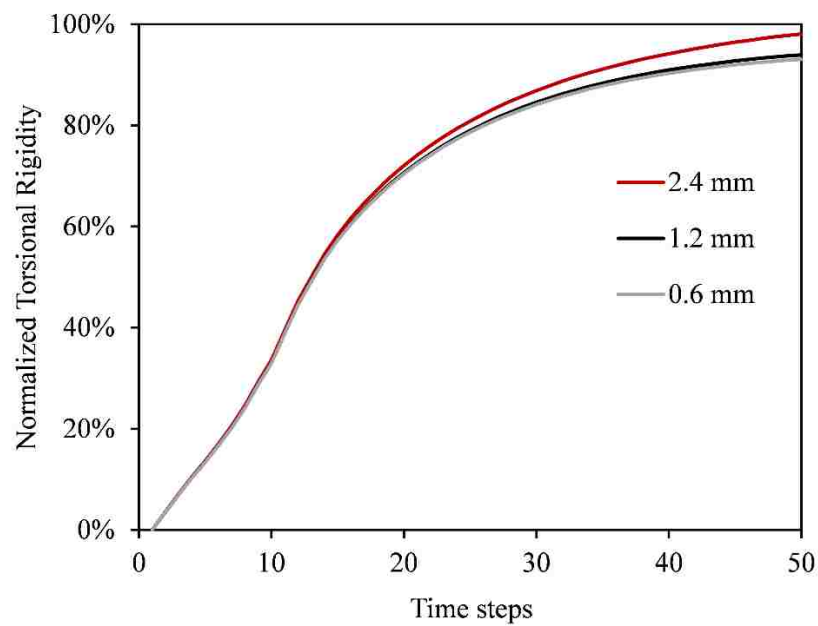
Figure 18. Progression of callus torsional rigidity for different mesh size.

Figure 17 shows that the results from the coarsest mesh size has a larger error compared to the others. Although the results accuracy improves as the mesh size becomes finer, the element number increased significantly, from 35098 to 211369, which in turn increased the time consuming of the 100 iterations from 8 hours to 21 hours. Based on this study, it was determined that the 1.2 mm mesh size is fine enough and less time consuming to complete the simulation.

4. Discussion

Overall, healing outcome in Figure 13 shows that even when all other factors were held constant (choice of implant, patient weight bearing, soft tissue injury and perfusion), the geometry of the fracture was also correlated with the interfragmentary strain, and thus can influence the healing outcome.

The results of this study also suggested that previously published fuzzy logic models for bone healing may require some parameter optimization to allow application in realistic fracture geometries with clinically relevant implant mechanics. The traditional fuzzy rules for distortional shear destructive cutoff (upper tissue formation limit) do not predict union with realistic geometries when torsion is applied, despite the fact that clinical nonunions are relatively rare in well-reduced, closed, simple (A) fractures [9]. One potential explanation for the predicted nonunions with the unadjusted mechanoregulation models is that this numerical modeling technique was originally developed and validated using axisymmetric models that were tuned by comparison to 2D histology sections and therefore may not adequately consider shear in a 3D environment. With our clinically relevant 3D geometries, replicating these simpler mechanical conditions by imposing no torsional load produced timely progress of healing, even in the unmodified model.

Notably, this is not the first study to incorporate torsional loading in a mechanoregulation model, but it is the first to demonstrate the difficulties we have observed pertaining to the cutoff for destructive distortional shear strain. One possible

explanation for this is that other investigators have modeled implant mechanics assuming external fixation, not intramedullary nailing, for the purposes of comparing predicted healing curves to existing *in vivo* datasets [33], [34]. In contrast, we have modeled implant mechanics based on direct test data from clinical nailing constructs because nailing is considered the gold standard method of fixation for diaphyseal tibial fractures in humans. The spurious nonunions that were predicted using the unadjusted mechanoregulation model would not have been observed without including free play arising from screw-hole dimensional clearances. The presence of a neutral zone or free-movement plateau in nailing constructs has been reported before [35], but rarely, with near ubiquitous reference to overall construct stiffness instead, which may have reinforced the acceptance of relatively low thresholds for destructive distortional shear throughout the literature.

The results presented here may have significant implications for mechanoregulation modeling of fracture healing processes. Specifically, this data suggests that *in vivo* bone healing may be somewhat less sensitive to distortional shear than the traditional models would predict. In this work, a higher upper boundary for the threshold of destruction of bone and cartilage during tissue differentiation was used in our fuzzy model to avoid spurious nonunion. However, this upper threshold for destruction was chosen to be arbitrarily high, rather than tuned to specific set point. A preponderance of preclinical and clinical evidence suggests that torsional instability should delay fracture healing and the models presented here do broadly concur with this conclusion, although the effect of torsion would likely be stronger if a valid new

distortion-mediated destructive shear threshold could be established. In this regard, continued reliance on model parameter tuning from ovine studies with external fixators is not likely to be fruitful and alternative clinical validation strategies, for example mechanical modeling from CT scan data [36] may be required.

This work also showed definitively—for the first time—that the rate of fracture healing depends on interfragmentary mechanics and is controlled in part by the fracture morphology, independent of all other factors. In these simulations, when all of the fuzzy rules were kept constant, changes in the fracture geometry produced different healing outcomes. These models represent a virtual experiment that is impossible to achieve clinically, in that the model parameters representing the choice of implant, patient weight bearing, and perfusion related to soft tissue injury were all controllable and constant. The results suggest that reported differences in the risk of clinical complications such as reoperation and nonunion in different to OTA/AO classification groups may actually reflect, at least in part, the underlying mechanical state of the interfragmentary healing zone.

Furthermore, this data confirms that torsional instability interferes with healing for all fracture geometries. Animal experimental data has repeatedly shown that healing is deficient with torsional instability compared to torsional rigidity. For example, use of an angle-stable tibial nail can help to reduce interfragmentary movements *in vivo* and thus lead to superior bone healing compared with standard tibial nailing [14]. Consequently, some decrease in healing rate with torsion should be expected, which

agrees well with our observation that torsional instability delays healing in mechanoregulated healing models across every AO/OTA fracture type considered.

This study and the results reported are subject to some important limitations:

I. The fracture healing process is a complex biological process that is regulated by both mechanical factors and biochemical factors. In this study, we only consider the regulatory role of mechanical stimuli on fracture healing. Biochemical factors, such as growth factors and perfusion change, also influent the healing process, are not considered in this model. Therefore, it will be an improvement for the current model to take the influence of biomechanical factors into account.

II. It is a numerical study which is accompanied with several modeling assumptions and experience data: One thing is that the load we applied was a simplified, and averaged loading scenario which cannot reflect the details of the patients' moving. The other thing is that in the fuzzy logic rules and functions. the simplest is the triangular membership function were used to model the fuzzy area of tissue destruction. The width of the fuzzy areas was also unvalidated by experiment data.

Finally, it is worth noting that a rule of mixtures was used in our model to calculate the Young's modulus and Poison's ratio for each of the finite elements. There are mainly two types of mixture rules in the published models: linear function or cubic function [24], [37], [38]. In the case of the elastic modulus, a linear rules of mixture is

known as the upper-bound modulus, and corresponds to loading parallel to the fiber tissues. In our model, we assumed that the newly generated tissue is stress oriented, which supports this linear mixture rule. Also, the rationale for cubic relation is weak, given that it is extrapolated from density-modulus regression relations in trabecular bone [38], rather than data specifically relevant to bone fracture callus. Nevertheless, the use of the cubic mixture rule mitigates the contribution of small bone percentages to the increase in local tissue stiffness, which would have the effect of delaying the decrease in strain that leads to favorable conditions for rapid bone formation. This may effectively delay healing in the simulation, which would in turn influence the optimization of tissue formation rates in previous papers [21], [24], leading to selection of rate constants that may be too fast to reflect realistic healing. Based on the above, we used linear rules in our model.

5. Conclusions

In summary, this is the first study of its kind to consider both fracture geometry and multi-axial loading (axial weight bearing with/without torsion) as relevant factors in the mechanoregulated bone healing processes. Compared to other models that used only transverse osteotomy fracture geometries, we used more realistic fracture geometries and showed that all types of fractures experience slower healing with torsional instability and may therefore benefit from increased torsional stability in fracture fixation when possible. Furthermore, we showed that mechanoregulation simulations are highly sensitive to distortional strain arising from torsional loading conditions and that previously published thresholds for destructive strain may be too low to predict healing in clinically realistic scenarios. Clinical fracture fixation by intramedullary nailing always includes some torsional instability, which has not been adequately represented in previous fuzzy logic models. To make these types of simulations more relevant, fuzzy rules need to be adapted to avoid predicting a nonunion that would not be expected in clinical practice.

Bibliography

[1]   M. B. Harris, "Rockwood and Green's fractures in adults, fifth edition," *Arthrosc. J. Arthrosc. Relat. Surg.*, vol. 18, no. 6, pp. 676–677, Jul. 2002.

[2]   R. Marsell and T. A. Einhorn, "The biology of fracture healing," *Injury*. 2011.

[3]   P. J. Prendergast, R. Huiskes, and K. Søballe, "Biophysical stimuli on cells during tissue differentiation at implant interfaces," *J. Biomech.*, 1997.

[4]   J. A. Bishop, A. A. Palanca, M. J. Bellino, and D. W. Lowenberg, "Assessment of Compromised Fracture Healing," *J. Am. Acad. Orthop. Surg.*, vol. 20, no. 5, pp. 273–282, May 2012.

[5]   E. Antonova, T. K. Le, R. Burge, and J. Mershon, "Tibia shaft fractures: costly burden of nonunions," *BMC Musculoskelet. Disord.*, vol. 14, no. 1, p. 42, Dec. 2013.

[6]   W.-H. Tay, R. de Steiger, M. Richardson, R. Gruen, and Z. J. Balogh, "Health outcomes of delayed union and nonunion of femoral and tibial shaft fractures," *Injury*, vol. 45, no. 10, pp. 1653–1658, Oct. 2014.

[7]   E. J. MacKenzie *et al.*, "Return to work following injury: the role of economic, social, and job-related factors.," *Am. J. Public Health*, vol. 88, no. 11, pp. 1630–1637, Nov. 1998.

[8]   K. Fong *et al.*, "Predictors of nonunion and reoperation in patients with fractures of the tibia: an observational study," *BMC Musculoskelet. Disord.*, vol. 14, no. 1, p. 103, Dec. 2013.

[9]   H. L. Dailey, K. A. Wu, P.-S. Wu, M. M. McQueen, and C. M. Court-Brown, "Tibial Fracture Nonunion and Time to Healing After Reamed Intramedullary Nailing," *J. Orthop. Trauma*, vol. 32, no. 7, pp. e263–e269, Jul. 2018.

[10]   K. O'Halloran *et al.*, "Will My Tibial Fracture Heal? Predicting Nonunion at the Time of Definitive Fixation Based on Commonly Available Variables," *Clin. Orthop. Relat. Res.*, vol. 474, no. 6, pp. 1385–1395, Jun. 2016.

[11]   D. R. Epari, J. P. Kassi, H. Schell, and G. N. Duda, "Timely fracture-healing requires optimization of axial fixation stability," *J. Bone Jt. Surg. - Ser. A*, vol. 89, no. 7, pp. 1575–1585, 2007.

[12]   H. Schell, D. R. Epari, J. P. Kassi, H. Bragulla, H. J. Bail, and G. N. Duda, "The course of bone healing is influenced by the initial shear fixation stability," *J. Orthop. Res.*, vol. 23, no. 5, pp. 1022–1028, Sep. 2005.

[13] P. Augat, J. Burger, S. Schorlemmer, T. Henke, M. Peraus, and L. Claes, "Shear movement at the fracture site delays healing in a diaphyseal fracture model," *J. Orthop. Res.*, vol. 21, no. 6, pp. 1011–1017, Nov. 2003.

[14] K. Kaspar *et al.*, "Angle stable locking reduces interfragmentary movements and promotes healing after unreamed nailing: Study of a displaced osteotomy model in sheep tibiae," *J. Bone Jt. Surg. - Ser. A*, vol. 87, no. 9 I, pp. 2028–2037, 2005.

[15] J. F. Kellam, E. G. Meinberg, J. Agel, M. D. Karam, and C. S. Roberts, "Introduction," *J. Orthop. Trauma*, vol. 32, no. 1, pp. S1–S10, 2018.

[16] L. E. Claes and C. A. Heigele, "Magnitudes of local stress and strain along bony surfaces predict the course and type of fracture healing," *J. Biomech.*, vol. 32, no. 3, pp. 255–266, 1999.

[17] C. Ament and E. P. Hofer, "A fuzzy logic model of fracture healing," *J. Biomech.*, vol. 33, no. 8, pp. 961–968, 2000.

[18] D. Lacroix and P. J. Prendergast, "A mechano-regulation model for tissue differentiation during fracture healing: Analysis of gap size and loading," *J. Biomech.*, vol. 35, no. 9, pp. 1163–1171, 2002.

[19] H. Isaksson, C. C. van Donkelaar, R. Huiskes, and K. Ito, "Corroboration of mechanoregulatory algorithms for tissue differentiation during fracture healing: comparison with in vivo results," *J. Orthop. Res.*, vol. 24, no. 5, pp. 898–907, Mar. 2006.

[20] L. Claes, P. Augat, G. Suger, and H. J. Wilke, "Influence of size and stability of the osteotomy gap on the success of fracture healing," *J. Orthop. Res.*, vol. 15, no. 4, pp. 577–584, 1997.

[21] U. Simon, P. Augat, M. Utz, and L. Claes, "A numerical model of the fracture healing process that describes tissue development and revascularisation," *Comput. Methods Biomech. Biomed. Engin.*, vol. 14, no. 1, pp. 79–93, 2011.

[22] M. Steiner, L. Claes, A. Ignatius, U. Simon, and T. Wehner, "Numerical simulation of callus healing for optimization of fracture fixation stiffness," *PLoS One*, vol. 9, no. 7, pp. 1–11, 2014.

[23] H. L. Dailey, D. Ph, C. J. Daly, and A. Glass-hardenbergh, "Mechanical Origins of Fracture Nonunion : Implant Tests and Finite Element Models of Callus Strains," 2015, p. 2.

[24] M. Wang and N. Yang, "Three-dimensional computational model simulating the fracture healing process with both biphasic poroelastic finite element analysis and fuzzy logic control," *Sci. Rep.*, no. April, pp. 1–13, 2018.

[25] E. N. Kubiak, M. J. Beebe, K. North, R. Hitchcock, and M. Q. Potter, "Early Weight Bearing After Lower Extremity Fractures in Adults," *J. Am. Acad. Orthop. Surg.*, vol. 21, no. 12, pp. 727–738, 2013.

[26] S. C. Gross, D. K. Galos, D. P. Taormina, A. Crespo, K. A. Egol, and N. C. Tejwani, "Can tibial shaft fractures bear weight after intramedullary nailing? A randomized controlled trial," *Journal of Orthopaedic Trauma*, vol. 30, no. 7. pp. 370–375, 2016.

[27] T. Wehner, L. Claes, and U. Simon, "Internal loads in the human tibia during gait," *Clin. Biomech.*, vol. 24, no. 3, pp. 299–302, 2009.

[28] S. J. Shefelbine, P. Augat, L. Claes, and U. Simon, "Trabecular bone fracture healing simulation with finite element analysis and fuzzy logic," *J. Biomech.*, vol. 38, no. 12, pp. 2440–2450, 2005.

[29] F. W. Rhinelander, "Tibial Blood Supply in Relation to Fracture Healing," *Clin. Orthop. Relat. Res.*, vol. 105, no. 1, p. 34???81, Nov. 1974.

[30] H. Isaksson, "Recent advances in mechanobiological modeling of bone regeneration," *Mechanics Research Communications*, vol. 42. pp. 22–31, 2012.

[31] M. Bottlang *et al.*, "Dynamic stabilization with active locking plates delivers faster, stronger, and more symmetric fracture-healing," *J. Bone Jt. Surg. - Am. Vol.*, vol. 98, no. 6, pp. 466–474, 2016.

[32] P. Augat, L. Claes, and K. Eckert-h, "The effect of mechanical stability on local vascularization and tissue differentiation in callus healing," *J. Orthop. Res.*, vol. 20, no. 5, pp. 1099–1105, 2002.

[33] M. Steiner, L. Claes, A. Ignatius, F. Niemeyer, U. Simon, and T. Wehner, "Prediction of fracture healing under axial loading, shear loading and bending is possible using distortional and dilatational strains as determining mechanical stimuli," *J. R. Soc. Interface*, vol. 10, no. 86, pp. 20130389–20130389, 2013.

[34] M. Steiner, L. Claes, A. Ignatius, U. Simon, and T. Wehner, "Disadvantages of interfragmentary shear on fracture healing - Mechanical insights through numerical simulation," *J. Orthop. Res.*, vol. 32, no. 7, pp. 865–872, 2014.

[35] R. Attal *et al.*, "The influence of distal locking on the need for fibular plating in intramedullary nailing of distal metaphyseal tibiofibular fractures," *Bone Jt. J.*, vol. 96 B, no. 3, pp. 385–389, 2014.

[36] P. Schwarzenberg, M. M. Maher, J. A. Harty, and H. L. Dailey, "Virtual structural analysis of tibial fracture healing from low-dose clinical CT scans," *J. Biomech.*, Nov. 2018.

[37] T. Wehner, M. Steiner, A. Ignatius, L. Claes, and C. M. Aegerter, "Prediction of the time course of callus stiffness as a function of mechanical parameters in experimental rat fracture healing studies - A numerical study," *PLoS One*, vol. 9, no. 12, pp. 1–16, 2014.

[38] H. W. Carter DR, "The Compressive Behaviour of Bone as a Two-Phase Porous Structure." J Bone Joint Surg Am, 1977.

Vita:

Tianyi Ren was born in Hefei, Anhui, PRC and grow up in Nanjing, Jiangsu, PRC. He enrolled at Southwest Jiaotong University in 2011 and completed his bachelor's degree in Mechanical Engineering in 2015. Tianyi was admitted in Lehigh University for graduate school.